Electronic Research Archive

https://www.aimspress.com/journal/era

ERA, 33(12): 7717–7735.
DOI: 10.3934/era.2025341
Received: 16 October 2025
Revised: 02 December 2025
Accepted: 08 December 2025
Published: 22 December 2025

Research article

A new result for numerical conformal mapping of bounded multiply connected domains

Jiayao Zhang[1], Yibin Lu[1,*], Yue Shan[1], Yingzi Wang[2] and Fuming Lai[3]

[1] Faculty of Science, Kunming University of Science and Technology, Kunming 650500, China
[2] Faculty of Information Engineering and Automation, Kunming University of Science and Technology, Kunming 650500, China
[3] School of Sustainable Energy and Materials Science, Jinhua Advanced Research Institute, Jinhua 321013, China

* **Correspondence:** Email: luyibin@kust.edu.cn.

Abstract: This paper proposes a novel numerical scheme based on an improved charge simulation method for computing conformal mappings of bounded multiply connected domains. The core of the method reformulates the mapping problem into a constraint system constructed via charge simulation. This system is then solved efficiently using the symmetric successive over-relaxation incomplete Cholesky conjugate gradient method, which is particularly well-suited for handling the ill-conditioned systems inherent to such problems. Numerical experiments show that our method achieves significantly higher accuracy and improved convergence rates compared to the conventional Gauss-Seidel iteration. The results confirm the robustness and practical potential of the proposed framework, establishing it as an efficient and reliable tool for computing conformal mappings of domains with high connectivity and complex geometry.

Keywords: charge simulation method; conformal mapping; bounded multiply connected domains; symmetric successive over-relaxation incomplete Cholesky conjugate gradient method; ill-conditioned systems

1. Introduction

Conformal mapping, a crucial technique in complex analysis and geometric processing, has various practical applications in engineering and science. These include hydrodynamics, engineering applications, image processing, electromagnetic theory, optics, and quantum mechanics [1, 2]. It is well-known that a conformal mapping function $w = f(z)$ can always be found from bounded multiply connected domains in the z-plane to canonical slit domains in the w-plane. However, problems in

practical applications tend to be more complex; we usually use numerical methods to approximate conformal mapping functions. Various numerical computational methods and applications have been proposed for conformal mapping functions on multiply connected domains [3, 4]. An integral equation method for conformal mapping based on Fredholm theory was proposed by Symm [5, 6]. This method can map simply connected domains onto a unit disk, as well as map the exterior of simply connected domains onto the exterior of a unit disk. Additionally, it can map doubly connected domains onto concentric annuli. Symm's method was simplified by Amano [7]. Amano [7] developed a set of algorithms based on the charge simulation method. The method maps simply connected domains onto unit disks and doubly connected regions onto concentric rings. Later, the algorithm also implements conformal mapping of multiply connected regions onto a variety of canonical slit domains applied to flow simulation problems [8–10]. Nasser et al. [11, 12] developed a unified method to calculate the conformal mapping functions of five classical Koebe canonical slit domains. This method, based on a boundary integral equation with a generalized Neumann kernel, is particularly suitable for solving conformal mapping problems in complex multiply connected domains. Crowdy [13] derived a generalized Schwarz-Christoffel mapping formula from bounded multiply connected circular domains to bounded multiply connected polygonal domains. Crowdy and Marshall [14] constructed explicit analytical formulas for conformal mappings from canonical multiply connected circular domains to canonical multiply connected slit domains by employing the Schottky-Klein prime function. Gu et al. [15] developed a universal framework for global conformal parameterization based on the cohomological structure of holomorphic one-forms, applicable to both bounded and unbounded surfaces. In subsequent work, Gu et al. [16] expanded their theoretical framework through additional computational methodologies, including harmonic mapping, Hodge decomposition, and meromorphic differential methods, with applications spanning computer graphics and medical imaging domains. Hakula et al. [17] and Hakula and Rasila [18] generalized the conjugate function method initially to multiply connected planar domains and subsequently to Riemann surfaces [17, 18].

In Nasser's approach, while the integral equation is well-conditioned, we typically prefer to avoid calculating complex integrals [19, 20]. Amano's charge simulation method transforms the conformal mapping problem into solving a two-dimensional Laplace boundary value problem [10]. First, a set of charge points is placed outside the problem domain to construct a linear combination of complex logarithmic functions approximating the conjugate harmonic function. Second, a corresponding matching point is assigned to each charge point, forming a system of constrained equations satisfying boundary conditions and regularization requirements. Solving this system determines the charge distribution and transformation radius. Amano's charge simulation method does not require the computation of integrals and uses the maximum modulus principle to evaluate errors, which has the advantages of short computation times, high computational accuracy, and avoidance of singular integrals. However, the system of constraint equations constructed by this method is ill-conditioned [9, 10]. Resolving these constraint equations is crucial for obtaining high accuracy charges and conformal mapping radius. Wang et al. [21] developed a parallel PCG algorithm and demonstrated its application to the 3D inversion of gravity-gradiometry data. Therefore, this paper proposes a new computational algorithm based on the charge simulation method for conformal mapping of bounded multiply connected domains to circular rings and disks with concentric arcs. The core contribution of this paper lies in proposing an innovative numerical algorithm based on an

improved charge simulation method for computing conformal mappings of bounded multiply connected domains. This novel algorithm not only stabilizes the solution process for the ill-conditioned systems in such problems but also significantly enhances computational efficiency and accuracy. Numerical experiments demonstrate that compared to the traditional Gauss-Seidel iteration method, this algorithm generates more accurate conformal mappings while substantially reducing the number of iterations required.

The rest of this paper is organized as follows: Section 2 describes the numerical conformal mapping of bounded multiply connected domains based on the charge simulation method. In Section 3, we propose a new algorithm based on the symmetric successive over-relaxation incomplete Cholesky conjugate gradient (SSOR-ICCG) method for numerical conformal mapping of multiply connected domains. Section 4 provides a method for configuring charge points and constraint points, and gives some numerical examples to show the superiority of the developed method. Conclusions are given in Section 5.

2. The charge simulation method for bounded multiply connected domains

In this section, we introduce the method of numerical conformal mapping from bounded multiply connected domains onto bounded canonical slit domains [10].

As shown in Figure 1, a bounded multiply connected domain D is bounded by closed Jordan curves $C_1, C_2, \ldots, C_n$, and $C_2, \ldots, C_n$ are surrounded by C_1. Without loss of generality, for the domain Ω_1, assume the mapping function $f(z)$ satisfies the normalizing condition $f(v) = 1$; for the domain Ω_2, assume the mapping function $f(z)$ satisfies the normalizing condition $f(u) = 0$ and $f(v) = 1$, where u and v are normalizing points. The curves S_1,S_2,... ,S_n are obtained after conformal mapping. The conformal mapping function $w = f(z)$ maps D to two types of bounded canonical slit domains where circular slit is unique.

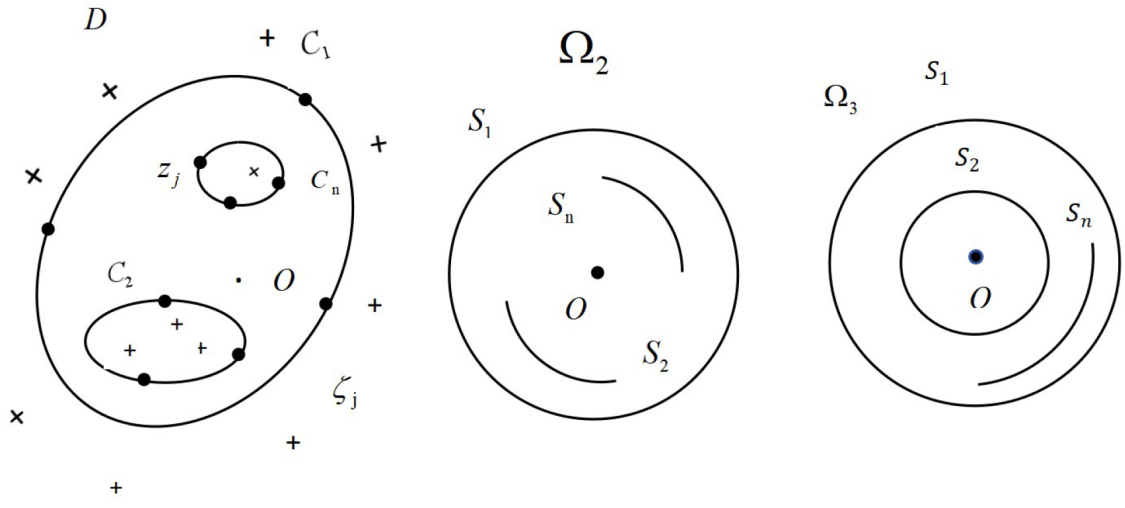

Figure 1. Conformal mappings from bounded multiply connected domains onto bounded canonical slit domains, where z_j and ζ_j are the collection points and the charge points, respectively.

The mapping functions onto bounded canonical domains can be expressed as

$$f(z) = (z-u)e^{(\psi(z)+i\phi(z))}, \tag{2.1}$$

where $\psi(z)$ and $\phi(z)$ are conjugate harmonic functions. $f(z)$ should satisfy the boundary condition $|f(z)| = r_l$ on C_l, $l = 1, 2, \ldots, N$. $r_1, r_2, \ldots, r_N$ are the radii of the circle and the circular slits. Based on the charge simulation method, $\psi(z)$ and $\phi(z)$ can be approximated by

$$\psi(z) + i\phi(z) \sim \Psi(z) + i\Phi(z) = Q_0 + \sum_{l=1}^{N}\sum_{j=1}^{N_l} Q_{lj}\log(z-\zeta_{lj}), \tag{2.2}$$

where Q_0 is a constant, $Q_{lj}(l = 1, 2, \ldots, N, j = 1, 2, \ldots, N_l)$ are charges, and $\zeta_{lj}(l = 1, 2, \ldots, N, j = 1, 2, \ldots, N_l)$ are charge points taken outside the given domain D. More precisely, $\zeta_{lj}(l = 1, 2, \ldots, N, j = 1, 2, \ldots, N_l)$ are arranged outside bounded by C_1 and inside the domain bounded by $C_m(m = 2, 3, \ldots, N)$ (see Figure 1).

The approximation of the harmonic function is used to satisfy the collocation boundary conditions:

$$\Psi(z_{mk}) = -\log|z_{mk} - u| + \log R_m, \tag{2.3}$$

where $z_{mk} \in C_m, m = 1, 2, \ldots, n, k = 1, 2, \ldots, N_m$, and $R_1, R_2, \ldots, R_N$ are the approximations of $r_1, r_2, \ldots, r_N$, respectively.

From the requirement of single-valuedness of the mapping, we obtain a restriction on $\Psi(z)$:

$$\begin{aligned}\int_{C_l} d\Psi(z) &= \int_{C_l} d\sum_{m=1}^{n}\sum_{j=1}^{N_m} Q_m \arg(z-\zeta_{mj}) \\ &= 2\pi\sum_{j=1}^{N_l} Q_{lj} = 0.l = 2, 3, \ldots, n.\end{aligned} \tag{2.4}$$

We also require that the approximate mapping function $F(z)$ should be invariant of scaling on the coordinate system for the problem domain D. From the single-valuedness condition Eq (2.4), we have

$$\sum_{l=1}^{N}\sum_{j=1}^{N_l} Q_{lj} = \sum_{j=1}^{N_1} Q_{1j} = -1. \tag{2.5}$$

From the normalizing condition $f(v) = 1$, we have

$$\Psi(v) + i\Phi(v) = Q_0 + \sum_{l=1}^{N}\sum_{j=1}^{N_l} Q_{lj}\log(v-\zeta_{lj}) = -\log(v-u). \tag{2.6}$$

Replace Q_0 with Eq (2.2), therefore:

$$\Psi(z) + i\Phi(z) = -\log(v-u) + \sum_{l=1}^{N}\sum_{j=1}^{N_l} Q_{lj}\log\left|\frac{z-\zeta_{lj}}{v-\zeta_{lj}}\right|. \tag{2.7}$$

From Eq (2.3), we have

$$\sum_{l=1}^{N}\sum_{j=1}^{N_l} Q_{lj}\log\left|\frac{z_{mk}-\zeta_{lj}}{v-\zeta_{lj}}\right| - \log R_m = -\log\left|\frac{z_{mk}-u}{v-u}\right|. \tag{2.8}$$

From Eqs (2.4), (2.5), and (2.8), we can construct a linear system, called the constraint equations, for numerical conformal mapping of bounded multiply connected domains based on the method of simulated charges. $Q_{lj}(l = 1, 2, \ldots, N, j = 1, 2, \ldots, N_l)$ and $\log R_l(l = 1, 2, \ldots, N)$ can be obtained by solving linear systems, then the approximate conformal mapping function can be expressed by

$$F(z) = \frac{z-u}{v-u} exp \sum_{l=1}^{N}\sum_{j=1}^{N_l} Q_{lj}\log\left|\frac{z-\zeta_{lj}}{v-\zeta_{lj}}\right|. \tag{2.9}$$

3. SSOR-ICCG method for numerical conformal mapping of bounded multiply connected domains

The location and number of charge points have a great influence on the coefficient matrix A of the constraint equations. For complex multiply connected domains, the condition number cond(A) of coefficient matrices is often large. That is to say, the coefficient matrix A is ill-conditioned. Therefore, it is important to find an effective method to solve the constraint equation to obtain high-precision charge points and conformal mapping radius. From Eqs (2.4), (2.5), and (2.8), the constraint equation can be written as

$$Ax = b, \tag{3.1}$$

where $A \in \mathrm{R}^{(\mathrm{N}+5)\times(\mathrm{N}+5)}$ is an asymmetric matrix, $b \in \mathrm{R}^{(\mathrm{N}+5)\times 1}$, and $x \in \mathrm{R}^{(\mathrm{N}+5)\times 1}$ is an unknown for Q_{lj} and $\log R_l$.

Consider the following preconditioned linear equations:

$$A^T Ax = A^T b. \tag{3.2}$$

Since A is non-singular, perform incomplete Cholesky factorization on matrix $A^T A$, yielding $A^T A = LL^T - R$, where L is a lower triangular matrix, R is the residual matrix, and $M = LL^T$ serves as the preconditioner matrix. Given that $M = LL^T \approx A^T A$, we obtain the preconditioned equivalent system of equations

$$Fy = g, \tag{3.3}$$

where $F = L^{-1}A^T AL^{-T}$, $y = L^T x$, and $g = L^{-1}A^T b$. The ICCG method proceeds as follows.

1) For $\forall x_0 \in \mathbb{R}^n$, calculate

$$\begin{aligned} r_0 &= A^T b - A^T Ax_0, \\ \tilde{r}_0 &= L^{-1} r_0, \\ p_0 &= L^{-T}\tilde{r}_0. \end{aligned}$$

2) For $k = 0, 1, 2, \cdots$, calculate

$$\begin{aligned} \alpha_k &= \frac{(\tilde{r}_k, \tilde{r}_k)}{(A^T A p_k, p_k)}, \\ x_{k+1} &= x_k + \alpha_k p_k, \\ \tilde{r}_{k+1} &= \tilde{r}_k - \alpha_k L^{-1} A^T A p_k. \end{aligned}$$

3) Calculate

$$\begin{aligned} \beta_k &= \frac{(\tilde{r}_{k+1}, \tilde{r}_{k+1})}{(\tilde{r}_k, \tilde{r}_k)}, \\ p_{k+1} &= L^{-T} \tilde{r}_{k+1} + \beta_k p_k. \end{aligned}$$

In the system of Eq (3.3), since matrix $A^T A$ is symmetric positive definite and so is F, when $M = LL^T$ approximates $A^T A$ more closely, F becomes closer to the identity matrix I. Consequently, the condition number of F approaches its minimum value of 1, leading to faster convergence of the ICCG method. In other words, the quality of the decomposition of the preconditioning matrix M directly affects the convergence behavior of the corresponding ICCG method.

For a symmetric positive definite matrix $A^T A$, we assume the matrix $A^T A$ can be decomposed into $A^T A = D - L_{A^T A} - L_{A^T A}^T$. Then the SSOR preconditioned matrix M is given by

$$\begin{aligned} M &= \frac{1}{\omega(2-\omega)} (D - \omega L_{A^T A}) D^{-1} (D - \omega L_{A^T A}^T) \\ &= LL^T, \end{aligned} \tag{3.4}$$

$$L = \frac{(D - \omega L_{A^T A}) D^{-1/2}}{\sqrt{\omega(2-\omega)}}, L^T = \frac{D^{-1/2}(D - \omega L_{A^T A}^T)}{\sqrt{\omega(2-\omega)}}, \tag{3.5}$$

where D is the diagonal matrix containing the diagonal elements of $A^T A$, $L_{A^T A}$ is the strictly negative lower triangular part of $A^T A$, and $\omega \in (0, 2)$ is the relaxation parameter.

From Eq (25) of [22],

$$\|x - x_k\|_A \leq 2 \left(\frac{\sqrt{\kappa_2(F)} - 1}{\sqrt{\kappa_2(F)} + 1} \right)^k \|x - x_0\|_A, \tag{3.6}$$

a small condition number of F leads to fast convergence, where $\kappa_2(F)$ is the condition number of F with respect to the 2-norm. By applying SSOR preconditioning with $M = LL^T$, the condition number of the transformed matrix F becomes approximately equal to the square root of the condition number of the original coefficient matrix $A^T A$ [23].

We integrate the SSOR decomposition method with the ICCG method by incorporating the factorization results from Eq (3.5), thus obtaining the SSOR-ICCG method [21]. According to previous analysis, the SSOR-ICCG method for numerical conformal mapping based on the charge simulation method can be summarized as follows.

In Algorithm 3.1, the parameters x_0, N, $ItMax$, ω, and ϵ are respectively defined as the zero vector, the number of charge points, the maximum number of iterations, relaxation factor, and error tolerance.

Algorithm 3.1 The SSOR-ICCG method for numerical conformal mapping.

Require: A, b, x_0, N, $ItMax$, ω, ϵ.

Ensure: the approximate conformal mapping function $F(z)$.

1: Give the place of charge points ζ_{li} and constraint points z_{li};
2: Construct the constraint equations $Ax = b$, calculate $A^TAx = A^Tb$;
3: Incomplete Cholesky factorization $A^TA = LL^T - R$;
4: Calculate $L = (D - \omega L_{A^TA})D^{-1/2}/\sqrt{\omega(2-\omega)}$, $L^T = D^{-1/2}(D - \omega L^T_{A^TA})/\sqrt{\omega(2-\omega)}$;
5: Initialize $r_0 = A^Tb - A^TAx_0$, $\tilde{r}_0 = L^{-1}r_0$, $p_0 = L^{-T}\tilde{r}_0$.
6: **while** $k < ItMax$ and $\|x_{k+1} - x_k\|_2 > \epsilon$ **do**
7: $\alpha_k = (\tilde{r}_k, \tilde{r}_k)/(A^TAp_k, p_k)$;
8: $x_{k+1} = x_k + \alpha_k p_k$;
9: $\tilde{r}_{k+1} = \tilde{r}_k - \alpha_k L^{-1}A^TAp_k$;
10: $\beta_k = (\tilde{r}_{k+1}, \tilde{r}_{k+1})/(\tilde{r}_k, \tilde{r}_k)$;
11: $p_{k+1} = L^{-T}\tilde{r}_{k+1} + \beta_k p_k$;
12: **end while**
13: Construct the approximate conformal mapping function $F(z)$;
14: **return** $F(z)$.

4. Numerical examples

In this section, we present the method of numerical conformal mappings from bounded multiply connected domains onto the bounded canonical slit domains. The experimental environment is Windows 10, MATLAB R2019a. In the numerical examples, we compare Gauss-Seidel method with our method. The conformal mapping error is estimated by

$$E_l = \max_j \left| |F(z_{lj+1/2})| - R_l \right|, \tag{4.1}$$

where $z_{lj+1/2} \in C_l$ is the middle point between points z_{lj} and z_{lj+1}, $l = 1, 2, 3, 4, 5$.

example 4.1. *The outer boundary is* $C_1 : |\frac{x}{a_1}| + |\frac{y}{b_1}| = 1$*, and the inner boundaries are* $C_l : |x - a_l| = d_l, |y - b_l| = d_l$*,* $l = 1, 2, 3, 4, 5$.

The constraint points z_{1j} on the diamond-shaped outer boundary C_1 are arranged by

$$z_{1j} = \frac{a_1 \cos\left(\frac{j\pi}{N_1}\right) + \mathrm{i}b_1 \sin\left(\frac{j\pi}{N_1}\right)}{\left|\cos\left(\frac{j\pi}{N_1}\right)\right| + \left|\sin\left(\frac{j\pi}{N_1}\right)\right|}, \tag{4.2}$$

and the charge points are placed by

$$\zeta_{1j} = \frac{a_1^* \cos\left(\frac{j\pi}{N_1}\right) + \mathrm{i}b_1^* \sin\left(\frac{j\pi}{N_1}\right)}{\left|\cos\left(\frac{j\pi}{N_1}\right)\right| + \left|\sin\left(\frac{j\pi}{N_1}\right)\right|}, \tag{4.3}$$

where $j \in [-N_1, N_1]$. For the inner boundaries $C_l (l = 2, 3, 4, 5)$, the constraint points are determined by

$$\begin{cases} x_{li} = d_l, \\ y_{li} = d_l \left(\dfrac{1 - r_{l(i-1)}}{1 - r_{lN_l}} \right). \end{cases} \tag{4.4}$$

The charge points are placed by

$$\begin{cases} \zeta_{li} = \left(1 - \dfrac{p_l}{q_l}\right)\left(d_l\left(\dfrac{1 - r_l^{i-1}}{1 - r_l^{N_l}}\right)\right) + p_l, \\ \zeta_{l(\frac{N_l}{8}+1)} = (q_l, q_l), \end{cases} \tag{4.5}$$

where $i = 1, 2, \cdots, \frac{N_l}{8}$. In numerical example 4.1, $a_1 = 4$, $b_1 = 2$, $a_1^* = 4.25$, $b_1^* = 2.2$, $a_2 = 0$, $a_3 = 1.65$, $a_4 = -1.65$, $a_5 = 1.2\mathrm{i}$, $b_2 = b_3 = b_4 = b_5 = 0$, $q_2 = q_3 = q_4 = q_5 = 0.99$, $p_2 = p_3 = p_4 = p_5 = 0.5$, $d_2 = 0.65$, $d_3 = d_4 = 0.45$, $d_5 = 0.25$, $u = 0$, $v = 3$, $\epsilon = 10^{-6}$, $ItMax = 1000$, $\omega = 1.5$, $r_2 = (\frac{1}{2})^{\left(\frac{8}{N_2-8}\right)}$, $r_3 = (\frac{1}{2})^{\left(\frac{8}{N_3-8}\right)}$, $r_4 = (\frac{1}{2})^{\left(\frac{8}{N_4-8}\right)}$, and $r_5 = (\frac{1}{2})^{\left(\frac{8}{N_5-8}\right)}$.

Figure 2 shows the distribution of charge points, where $N_1 = 64$ charge points are placed outside boundary C_1; similarly, $N_2 = N_3 = N_4 = N_5 = 64$ points are placed inside boundaries C_2, C_3, C_4, and C_5, respectively. The numerical results are shown in Figure 3 for various values of $N = N_1 + N_2 + N_3 + N_4 + N_5$, GS_1, GS_2, GS_3, GS_4, and GS_5 represent the error of the Gauss-Seidel method, and SI_1, SI_2, SI_3, SI_4, and SI_5 represent the error of the SSOR-ICCG method. From Figure 3, it is evident that the conformal mapping error of the proposed method is smaller than that of the Gauss-Seidel method, which means that this method can be constructed with higher precision approximate conformal mapping functions $F(z)$.

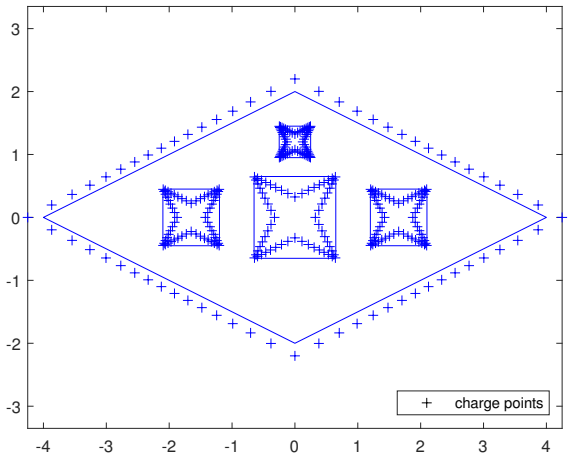

Figure 2. Place of charge points for example 4.1.

Some numerical results are listed in Table 1 for comparison. In Table 1, ItMaxG and ItMaxS are respectively defined as the maximum number of iterations of the Gauss-Seidel method and the maximum number of iterations of the SSOR-ICCG method. For N=320, the proposed algorithm achieved an error of 6.61×10^{-4} in 1000 iterations, demonstrating a substantial improvement over the Gauss-Seidel method, which required 3000 iterations to attain an error of 1.45×10^{-1}. In Figure 4, the thick solid lines represent the boundaries, and the thin lines represent the contour lines. By using the SSOR-ICCG method to calculate the constraint equations to obtain charges Q_{lj}, we then construct the approximate conformal mapping function $F(z)$. The function $F(z)$ maps the domain of Figure 4 into circular rings with concentric arcs shown in Figure 5. From Figure 5, the method used in this paper demonstrates its effectiveness.

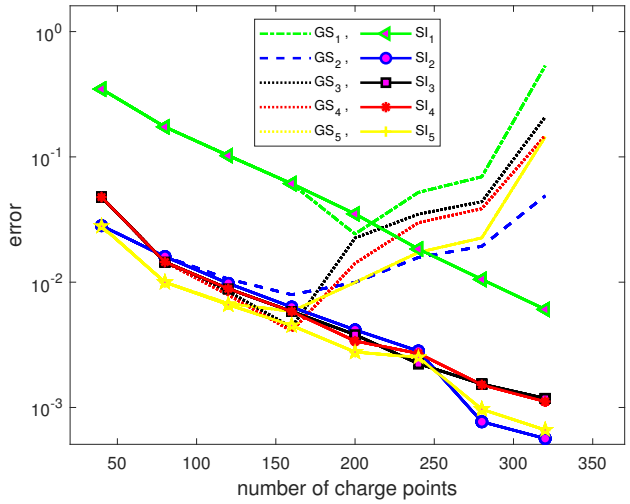

Figure 3. Error curves for example 4.1.

Table 1. Comparison of numerical conformal mapping error and iteration number (example 4.1).

N	GS_1	GS_2	GS_3	GS_4	GS_5	**ItMaxG**	SI_1	SI_2	SI_3	SI_4	SI_5	**ItMaxS**
40	3.48×10^{-1}	2.82×10^{-2}	4.77×10^{-2}	4.77×10^{-2}	2.80×10^{-2}	**687**	3.48×10^{-1}	2.82×10^{-2}	4.77×10^{-2}	4.77×10^{-2}	2.80×10^{-2}	**70**
80	1.74×10^{-1}	1.60×10^{-2}	1.45×10^{-2}	1.45×10^{-2}	1.00×10^{-2}	**2180**	1.74×10^{-1}	1.60×10^{-2}	1.45×10^{-2}	1.45×10^{-2}	1.00×10^{-2}	**182**
120	1.03×10^{-1}	1.06×10^{-2}	8.40×10^{-3}	7.90×10^{-3}	6.80×10^{-3}	**3000**	1.02×10^{-1}	9.80×10^{-3}	8.90×10^{-3}	8.90×10^{-3}	6.60×10^{-3}	**347**
160	6.10×10^{-2}	8.00×10^{-3}	4.40×10^{-3}	4.10×10^{-3}	5.90×10^{-3}	**3000**	6.12×10^{-2}	6.30×10^{-3}	5.80×10^{-3}	5.80×10^{-3}	4.50×10^{-3}	**715**
200	2.42×10^{-2}	1.00×10^{-2}	2.25×10^{-2}	1.41×10^{-2}	1.00×10^{-2}	**3000**	3.51×10^{-2}	4.20×10^{-3}	3.80×10^{-3}	3.40×10^{-3}	2.80×10^{-3}	**1000**
240	5.21×10^{-2}	1.58×10^{-2}	3.49×10^{-2}	2.98×10^{-2}	1.73×10^{-2}	**3000**	1.84×10^{-2}	2.80×10^{-3}	2.20×10^{-3}	2.70×10^{-3}	2.50×10^{-3}	**1000**
280	6.94×10^{-2}	1.93×10^{-2}	4.39×10^{-2}	3.86×10^{-2}	2.26×10^{-2}	**3000**	1.05×10^{-2}	7.69×10^{-4}	1.50×10^{-3}	1.50×10^{-3}	9.68×10^{-4}	**1000**
320	5.32×10^{-1}	4.89×10^{-2}	2.08×10^{-1}	1.48×10^{-1}	1.45×10^{-1}	**3000**	6.10×10^{-3}	5.65×10^{-4}	1.20×10^{-3}	1.10×10^{-3}	6.61×10^{-4}	**1000**

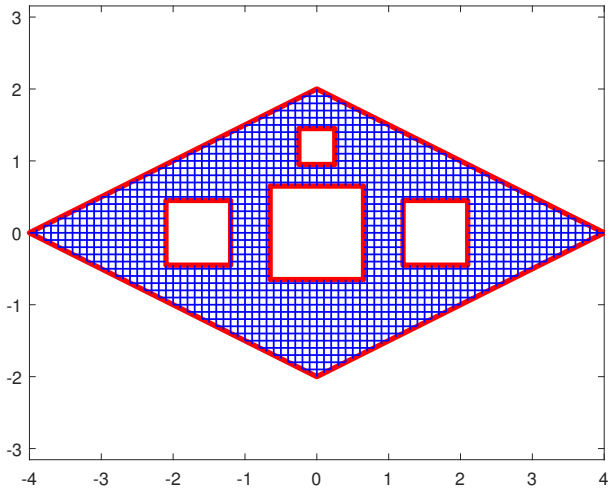

Figure 4. The contour lines for example 4.1.

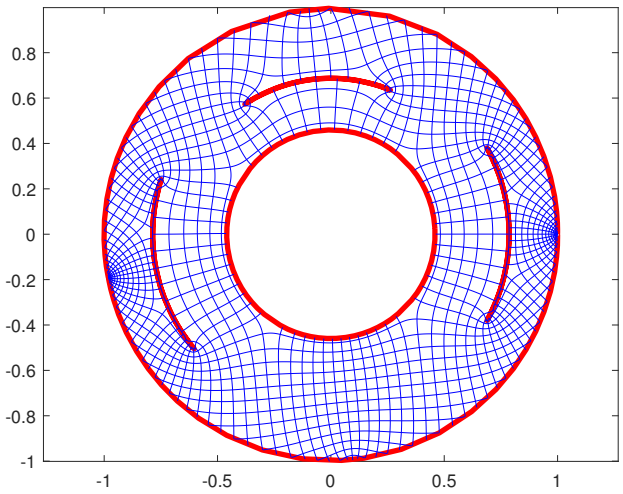

Figure 5. The image is mapped for example 4.1.

example 4.2. *The outer boundary is* $C_1 : \frac{x^2}{a^2} + \frac{y^2}{b^2} = 1$, *and the inner boundaries are* $C_l : \{z||z - z_{0l}| = \gamma_l\}$, $l = 2, 3, 4, 5$.

Consider the outer boundary of the ellipse, denoted as C_1. The constraint points z_{1j} are arranged by

$$z_{1j} = a\cos\left(\frac{j\pi}{N}\right) + \mathrm{i}b\sin\left(\frac{j\pi}{N}\right), \tag{4.6}$$

$$\zeta_{1j} = 1.5a\cos\left(\frac{j\pi}{N}\right) + \mathrm{i}\frac{5}{3}\sin\left(\frac{j\pi}{N}\right). \tag{4.7}$$

For the inner boundaries $C_l(l = 2, 3, 4, 5)$, the constraint points z_{lj} and charge points ζ_{lj} are determined by Figure 6,

$$z_{lj} = z_{0l} + \gamma_l\left(\cos\left(\frac{j\pi}{N}\right) + \mathrm{i}\sin\left(\frac{j\pi}{N}\right)\right), \tag{4.8}$$

and

$$\zeta_{lj} = z_{0l} + \beta\gamma_l\left(\cos\left(\frac{j\pi}{N}\right) + \mathrm{i}\sin\left(\frac{j\pi}{N}\right)\right), \tag{4.9}$$

where $j \in [-N, N]$, and $0 < \beta < 1$ is a parameter for the charge placement for the inner boundaries $C_l(l = 2, 3, 4, 5)$.

In numerical example 4.2, $a = 3.7$, $b = 1$, $\beta = 0.5$, $z_{02} = 1$, $z_{03} = -0.8$, $z_{04} = 2.5$, $z_{05} = -2.5$, $\gamma_2 = \gamma_4 = 0.6$, $\gamma_3 = \gamma_5 = 0.5$, $u = 0$, $v = 3$, $\epsilon = 10^{-6}$, $ItMax = 2000$, and $\omega = 1.5$.

Figure 6 shows the distribution of charge points. The numerical results are shown in Figure 7. From Figure 7, the error of the conformal mapping obtained by this method is significantly smaller than that of the Gauss-Seidel method.

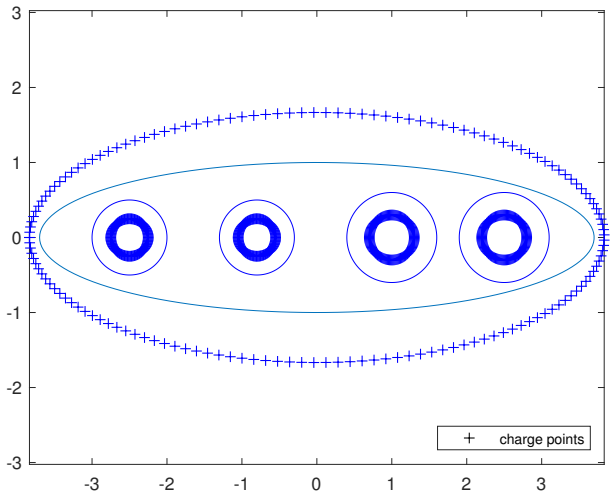

Figure 6. Place of charge points for example 4.2.

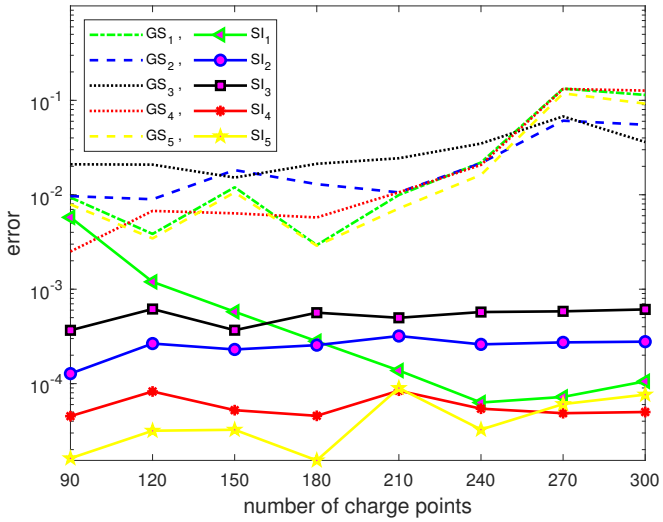

Figure 7. Error curves for example 4.2.

In Table 2, for N=300, the error and iteration count for GS_1 were 2.90×10^{-3} and 8000, respectively, while those for SI_1 were 1.54×10^{-5} and 1605. Our method yields both a significantly smaller error and requires considerably fewer iterations than the Gauss-Seidel method. In Figure 8, the thick solid lines represent the boundaries, and the thin lines represent the contour lines. By using our method to calculate the constraint equations to obtain charges Q_{lj}, we then construct the approximate conformal mapping function $F(z)$. The function $F(z)$ maps the domain of Figure 8 into circular disks with concentric arcs shown in Figure 9. From Figure 9, the method proposed in this paper validates its effectiveness.

example 4.3. *The outer boundary is* $C_1 : x^2 + y^2 + ay = a\sqrt{x^2 + y^2}(a > 0)$, *and the inner boundaries are* $C_l : \{z||z - z_{0l}| = \gamma_l\}$, $l = 2, 3, 4, 5$.

Table 2. Comparison of numerical conformal mapping error and iteration number (example 4.2).

N	GS_1	GS_2	GS_3	GS_4	GS_5	**ItMaxG**	SI_1	SI_2	SI_3	SI_4	SI_5	**ItMaxS**
90	9.40×10^{-3}	9.70×10^{-3}	2.10×10^{-2}	2.50×10^{-3}	7.90×10^{-3}	**8000**	5.80×10^{-3}	1.28×10^{-4}	3.67×10^{-4}	4.52×10^{-5}	1.62×10^{-5}	**2000**
120	3.80×10^{-3}	9.00×10^{-3}	2.08×10^{-2}	6.70×10^{-3}	3.40×10^{-3}	**8000**	1.20×10^{-3}	2.66×10^{-4}	6.17×10^{-4}	8.26×10^{-5}	3.17×10^{-5}	**1160**
150	1.20×10^{-2}	1.83×10^{-2}	1.52×10^{-2}	6.40×10^{-3}	1.06×10^{-2}	**8000**	5.77×10^{-4}	2.30×10^{-4}	3.68×10^{-4}	5.23×10^{-5}	3.25×10^{-5}	**1756**
180	2.90×10^{-3}	1.29×10^{-2}	2.13×10^{-2}	5.70×10^{-3}	2.90×10^{-3}	**8000**	2.81×10^{-4}	2.56×10^{-4}	5.64×10^{-4}	4.56×10^{-5}	1.54×10^{-5}	**1605**
210	9.90×10^{-3}	1.06×10^{-2}	2.44×10^{-2}	1.06×10^{-2}	7.20×10^{-3}	**8000**	1.38×10^{-4}	3.19×10^{-4}	4.98×10^{-4}	8.42×10^{-5}	8.98×10^{-5}	**2000**
240	2.20×10^{-2}	2.16×10^{-2}	3.49×10^{-2}	2.07×10^{-2}	1.62×10^{-2}	**8000**	6.31×10^{-5}	2.60×10^{-4}	5.73×10^{-4}	5.42×10^{-5}	3.26×10^{-5}	**1837**
270	1.33×10^{-1}	6.09×10^{-2}	6.75×10^{-2}	1.32×10^{-1}	1.19×10^{-1}	**8000**	7.23×10^{-5}	2.73×10^{-4}	5.83×10^{-4}	4.86×10^{-5}	6.07×10^{-5}	**1804**
300	1.14×10^{-1}	5.52×10^{-2}	3.62×10^{-2}	1.27×10^{-1}	9.22×10^{-2}	**8000**	1.06×10^{-4}	2.78×10^{-4}	6.11×10^{-4}	5.00×10^{-5}	7.65×10^{-5}	**1896**

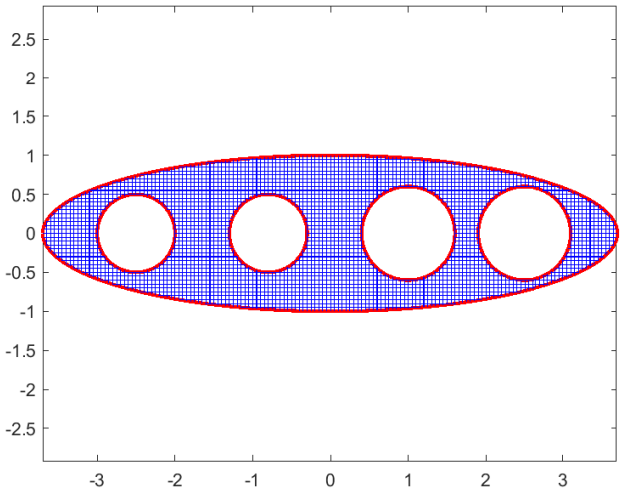

Figure 8. The contour lines for example 4.2.

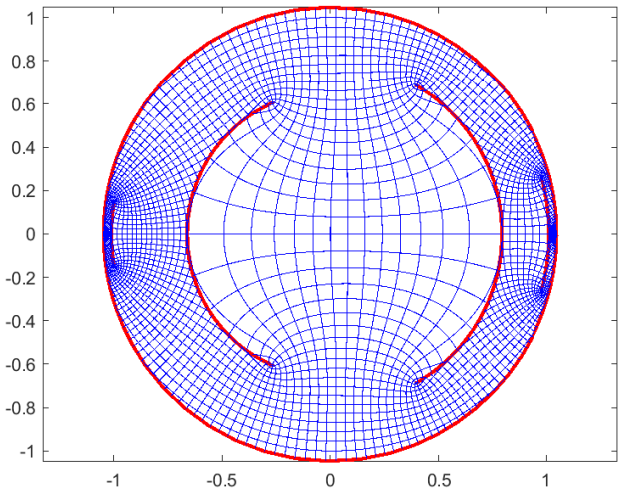

Figure 9. The image is mapped for example 4.2.

For the outer boundary, C_1 consists of a cardioid translated upwards along the y-axis by β units, where $\beta = \frac{1}{2} \mid y_{\max} + y_{\min} \mid$, $y_{\max}$, and $y_{\min}$ denote the maximum and minimum values of y, respectively. The constraint points z_{1j} are arranged by:

$$\begin{cases} x_j = a\left(\sin(\frac{j\pi}{N}) - 0.5\sin(\frac{2j\pi}{N})\right), \\ y_j = a\left(\cos(\frac{j\pi}{N}) - \cos^2(\frac{j\pi}{N})\right) + \alpha. \end{cases} \tag{4.10}$$

Charge points ζ_{1j} are distributed over the outer boundary C_1, and the position is determined by

$$\zeta_{1j} = \lambda a\left(\sin(\frac{j\pi}{N}) - 0.5\sin(\frac{2j\pi}{N})\right) + \mathrm{i}\left(\lambda a\left(\cos(\frac{j\pi}{N}) - \cos^2(\frac{j\pi}{N})\right) + \alpha\right), \tag{4.11}$$

where $j \in [-N, N]$, and $\lambda > 1$ is a parameter for the charge placement for the outer boundary C_1.

For the inner boundaries $C_l (l = 2, 3, 4, 5)$, the constraint points z_{lj} and charge points ζ_{lj} are determined by Eqs (4.8) and (4.9).

In numerical example 4.3 , $\lambda = 1.5$, $a = 1.3$, $\beta = 0.5$, $z_{02} = 0$, $z_{03} = 1.2$, $z_{04} = -1.2$, $z_{05} = -\mathrm{i}$, $\gamma_2 = 0.5$, $\gamma_3 = \gamma_4 = \gamma_5 = 0.3$, $u = 0$, $v = 1.6846$, $\epsilon = 10^{-6}$, $ItMax = 2000$, and $\omega = 1.5$.

Similar to Figures 6 and 7, Figure 10 shows the distribution of charge points. The numerical results are shown in Figure 11. From Figure 11, it is evident that the conformal mapping error of the proposed method is smaller than that of the Gauss-Seidel method. By using the SSOR-ICCG method to calculate the constraint equations to obtain the charges Q_{lj}, we then construct the approximate conformal mapping function $F(z)$.

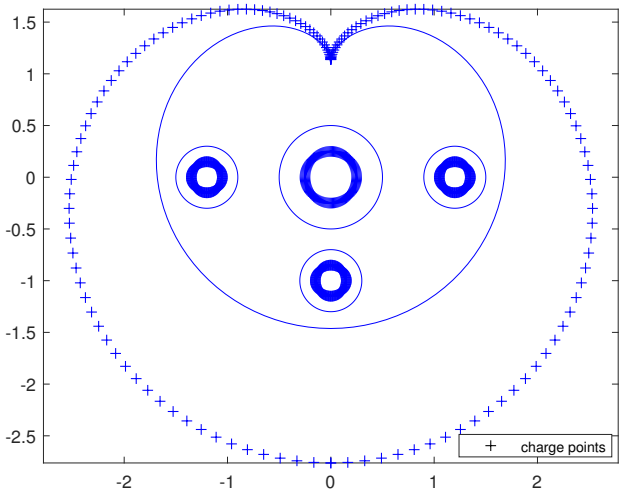

Figure 10. Place of charge points for example 4.3.

In Table 3. The iteration numbers of the Gauss-Seidel method are larger than those of our method. In Figure 12, the thick solid lines represent the boundaries, and the thin lines represent the contour lines. The function $F(z)$ maps the domain of Figure 12 into circular rings with concentric arcs shown in Figure 13. From Figure 13, the method used in this paper demonstrates its effectiveness.

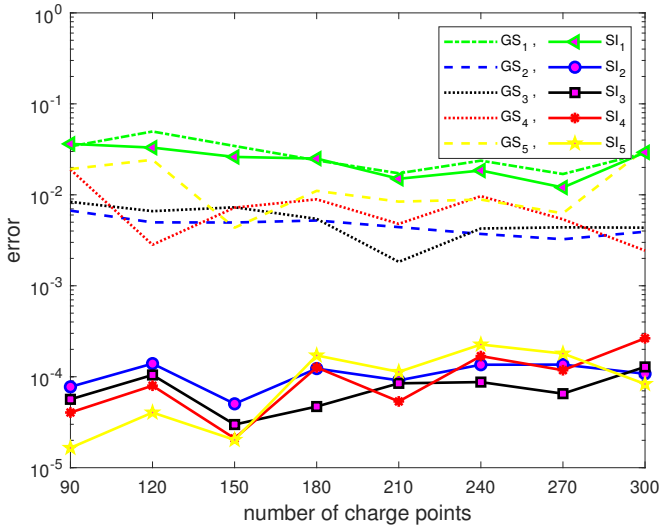

Figure 11. Error curves for example 4.3.

Table 3. Comparison of numerical conformal mapping error and iteration number (example 4.3).

N	GS_1	GS_2	GS_3	GS_4	GS_5	**ItMaxG**	SI_1	SI_2	SI_3	SI_4	SI_5	**ItMaxS**
90	3.41×10^{-2}	6.70×10^{-3}	8.40×10^{-3}	1.90×10^{-2}	1.92×10^{-2}	**3000**	3.63×10^{-2}	7.74×10^{-5}	5.65×10^{-5}	4.04×10^{-5}	1.65×10^{-5}	**1348**
120	4.97×10^{-2}	5.00×10^{-3}	6.60×10^{-3}	2.80×10^{-3}	2.43×10^{-2}	**3000**	3.30×10^{-2}	1.39×10^{-4}	1.05×10^{-4}	7.97×10^{-5}	4.04×10^{-5}	**611**
150	3.44×10^{-2}	5.00×10^{-3}	7.30×10^{-3}	7.20×10^{-3}	4.40×10^{-3}	**3000**	2.61×10^{-2}	5.04×10^{-5}	2.98×10^{-5}	2.10×10^{-5}	2.02×10^{-5}	**1906**
180	2.39×10^{-2}	5.20×10^{-3}	5.40×10^{-3}	8.90×10^{-3}	1.11×10^{-2}	**3000**	2.50×10^{-2}	1.23×10^{-4}	4.70×10^{-5}	1.26×10^{-4}	1.71×10^{-4}	**2000**
210	1.72×10^{-2}	4.40×10^{-3}	1.80×10^{-3}	4.80×10^{-3}	8.40×10^{-3}	**3000**	1.50×10^{-2}	9.12×10^{-5}	8.46×10^{-5}	5.35×10^{-5}	1.13×10^{-4}	**2000**
240	2.37×10^{-2}	3.70×10^{-3}	4.30×10^{-3}	9.70×10^{-3}	8.90×10^{-3}	**3000**	1.85×10^{-2}	1.36×10^{-4}	8.73×10^{-5}	1.69×10^{-4}	2.26×10^{-4}	**2000**
270	1.69×10^{-2}	3.20×10^{-3}	4.40×10^{-3}	5.40×10^{-3}	6.30×10^{-3}	**3000**	1.20×10^{-2}	1.36×10^{-4}	6.52×10^{-5}	1.18×10^{-4}	1.80×10^{-4}	**2000**
300	2.88×10^{-2}	3.90×10^{-3}	4.40×10^{-3}	2.40×10^{-3}	3.18×10^{-2}	**3000**	2.93×10^{-2}	1.08×10^{-4}	1.28×10^{-4}	2.65×10^{-4}	8.33×10^{-5}	**2000**

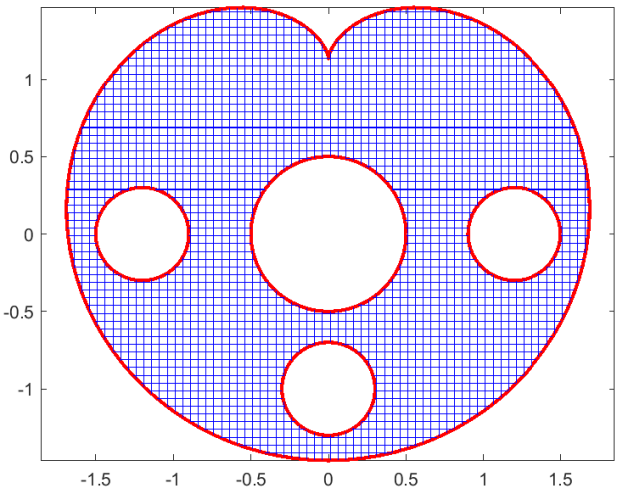

Figure 12. The contour lines for example 4.3.

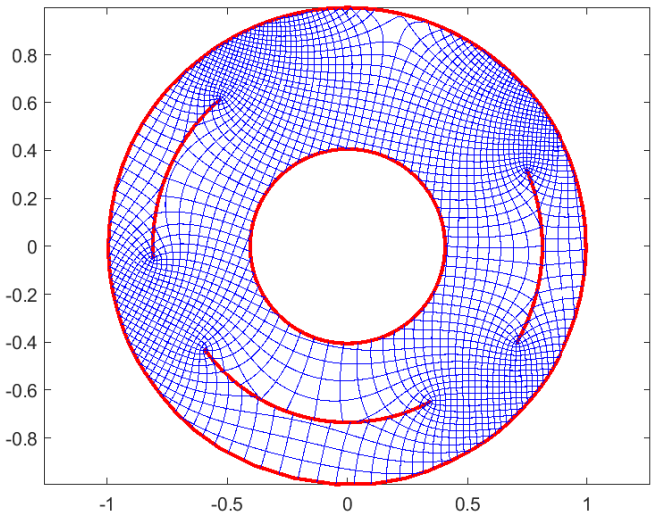

Figure 13. The image is mapped for example 4.3.

example 4.4. *The outer boundary is* $C_1 : x^{2/3} + y^{2/3} = b^{2/3}(b > 0)$*, and the inner boundaries are* $C_l : \{z||z - z_{0l}| = \gamma_l\}$, $l = 2, 3, 4, 5$.

This example has been considered for the outer boundary C_1 of tetracuspid. The constraint points z_{1j} are arranged by

$$\begin{cases} x_j = b\sin^3(\frac{\pi j}{N}), \\ y_j = b\cos^3(\frac{\pi j}{N}), \end{cases} \tag{4.12}$$

and the charge points are placed by

$$\zeta_{1j} = \lambda b\left(\sin^3(\frac{\pi j}{N}) + \cos^3(\frac{\pi j}{N})\right), \tag{4.13}$$

where $j \in [-N, N]$. For the inner boundaries $C_l(l = 2, 3, 4, 5)$, the constraint points z_{lj} and charge points ζ_{lj} are determined by Eq (4.8) and (4.9).

In numerical example 4.4, $\lambda = 1.1$, $b = 3$, $\beta = 0.5$, $z_{02} = 1.1$, $z_{03} = -1.1$, $z_{04} = 1.1\times\mathrm{i}$, $z_{05} = -1.1\times\mathrm{i}$, $\gamma_2 = \gamma_3 = \gamma_4 = \gamma_5 = 0.6$, $u = 0$, $v = 3$, $\epsilon = 10^{-6}$, $ItMax = 2000$, and $\omega = 1.5$.

Figure 14 shows the distribution of charge points. The numerical results for this example are shown in Figure 15, and some numerical results are listed in Table 4 for comparison. As can be seen from Figure 15, our method can achieve higher accuracy compared to the Gauss-Seidel method. In Figure 16, the thick solid lines represent the boundaries, and the thin lines represent the contour lines. In Figure 16 and Figure 17, $F(z)$ maps C_1 onto the unit circle and maps C_2 and C_3 onto circular arc slits of different sizes.

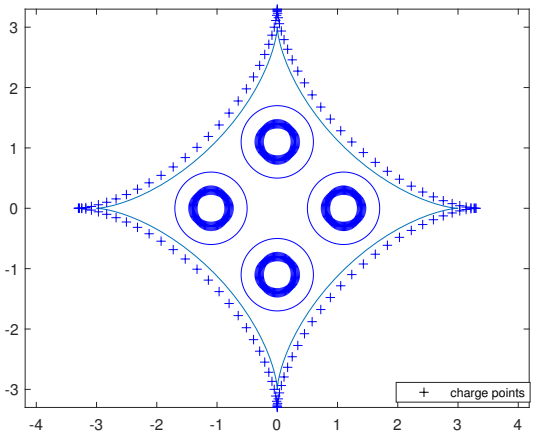

Figure 14. Place of charge points for example 4.4.

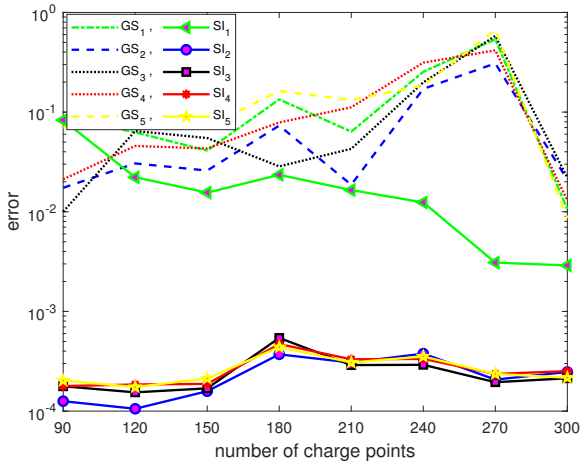

Figure 15. Error curves for example 4.4.

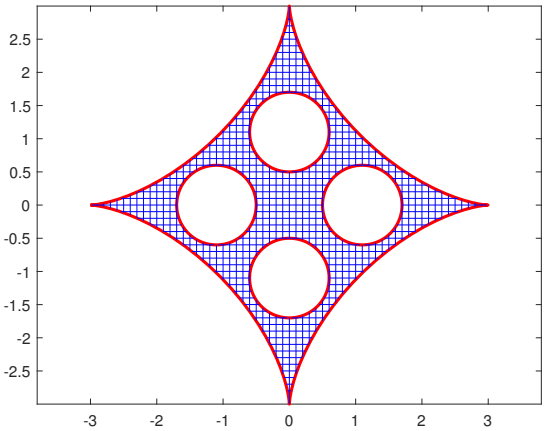

Figure 16. The contour lines for for example 4.4.

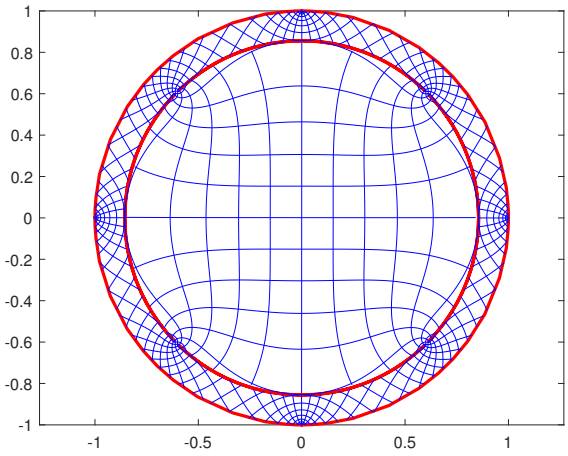

Figure 17. The image is mapped for example 4.4.

In Table 4, the iteration number of the Gauss-Seidel method is larger than that of our method. Using the SSOR-ICCG method to solve the constraint equations, we obtain the charges Q_{lj} and construct the approximate conformal mapping function $F(z)$. This function maps the domain of Figure 16 to circular disks with concentric arcs. As shown in Figure 17, the method used in this paper is effective.

Table 4. Comparison of numerical conformal mapping error and iteration number (example 4.4).

N	GS_1	GS_2	GS_3	GS_4	GS_5	**ItMaxG**	SI_1	SI_2	SI_3	SI_4	SI_5	**ItMaxS**
90	8.94×10^{-2}	1.74×10^{-2}	1.00×10^{-2}	2.12×10^{-2}	7.04×10^{-2}	**8000**	8.94×10^{-2}	1.26×10^{-4}	1.77×10^{-4}	1.78×10^{-4}	2.03×10^{-4}	**2000**
120	6.27×10^{-2}	3.06×10^{-2}	6.46×10^{-2}	4.57×10^{-2}	7.15×10^{-2}	**8000**	6.27×10^{-2}	1.06×10^{-4}	1.54×10^{-4}	1.85×10^{-4}	1.74×10^{-4}	**2000**
150	4.11×10^{-2}	2.59×10^{-2}	5.49×10^{-2}	4.32×10^{-2}	7.13×10^{-2}	**8000**	4.11×10^{-2}	1.58×10^{-4}	1.69×10^{-4}	1.88×10^{-4}	2.13×10^{-4}	**2000**
180	1.34×10^{-1}	7.32×10^{-2}	2.85×10^{-2}	7.87×10^{-2}	1.63×10^{-1}	**8000**	1.34×10^{-1}	3.71×10^{-4}	5.42×10^{-4}	4.71×10^{-4}	4.38×10^{-4}	**2000**
210	6.37×10^{-2}	1.87×10^{-2}	4.28×10^{-2}	1.12×10^{-1}	1.32×10^{-1}	**8000**	6.37×10^{-2}	3.07×10^{-4}	2.9×10^{-4}	3.31×10^{-4}	3.08×10^{-4}	**2000**
240	2.54×10^{-1}	1.71×10^{-1}	1.99×10^{-1}	3.13×10^{-1}	1.85×10^{-1}	**8000**	2.54×10^{-1}	3.77×10^{-4}	2.92×10^{-4}	3.34×10^{-4}	3.53×10^{-4}	**2000**
270	5.38×10^{-1}	3.08×10^{-1}	5.81×10^{-1}	4.17×10^{-1}	6.67×10^{-1}	**8000**	5.38×10^{-1}	2.07×10^{-4}	1.95×10^{-4}	2.36×10^{-4}	2.36×10^{-4}	**2000**
300	1.06×10^{-2}	2.10×10^{-2}	2.20×10^{-2}	1.30×10^{-2}	8.60×10^{-3}	**8000**	1.06×10^{-2}	2.47×10^{-4}	2.14×10^{-4}	2.52×10^{-4}	2.16×10^{-4}	**2000**

5. Conclusions

This paper presents an innovative numerical method based on an improved charge simulation approach for computing conformal mappings of bounded multiply connected domains. At its core, the method transforms the mapping problem into a constrained system of equations constructed via the charge simulation method, which is then solved efficiently and stably using the SSOR-ICCG method for handling ill-conditioned systems. Extensive numerical experiments validate the superiority of the proposed method. Compared to the traditional Gauss-Seidel method, our algorithm significantly reduces computational error and greatly improves convergence efficiency, demonstrating its robustness and practical value. Looking ahead, while the proposed method is not applicable to conformal mappings of canonical slit domains of the fifth type, identifying alternative effective approaches to address this limitation represents an important direction for future research.

Furthermore, more refined error metrics, such as the reciprocal error [24], will be introduced to enable a comprehensive and rigorous evaluation of mapping accuracy.

Use of AI tools declaration

The authors declare they have not used Artificial Intelligence (AI) tools in the creation of this article.

Acknowledgments

This work is supported by the National Natural Science Foundation of China (No. 12461079) and the Kunming University of Science and Technology Interdisciplinary Research Project (No. KUST-xk202025016).

Conflict of interest

The authors declare there is no conflict of interest.

References

1. D. Crowdy, Conformal slit maps in applied mathematics, *Anziam J.*, **53** (2012), 171–189. https://doi.org/10.1017/S1446181112000119
2. K. He, J. Chang, D. Pang, B. Sun, Z. Yin, D. Li, Iterative algorithm for the conformal mapping function from the exterior of a roadway to the interior of a unit circle, *Arch. Appl. Mech.*, **92** (2022), 971–991. https://doi.org/10.1007/s00419-021-02087-w
3. D. Ntalampekos, Rigidity and continuous extension for conformal maps of circle domains, *Trans. Am. Math. Soc.*, **376** (2023), 5221–5239. https://doi.org/10.1090/tran/8923
4. T. Bergamaschi, W. I. Jay, P. R. Oare, Hadronic structure, conformal maps, and analytic continuation, *Phys. Rev. D* , **108** (2023), 074516, https://doi.org/10.1103/PhysRevD.108.074516
5. G. T. Symm, An integral equation method in conformal mapping, *Numer. Math.*, **9** (1966), 250–258. https://doi.org/10.1007/bf02162088
6. G. T. Symm, Conformal mapping of doubly-connected domains, *Numer. Math.*, **13** (1969), 448–457. https://doi.org/10.1007/bf02163272
7. K. Amano, A charge simulation method for the numerical conformal mapping of interior, exterior and doubly-connected domains, *J. Comput. Appl. Math.*, **53** (1994), 353–370. https://doi.org/10.1016/0377-0427(94)90063-9
8. D. Okano, H. Ogata, K. Amano, M. Sugihara, Numerical conformal mappings of bounded multiply connected domains by the charge simulation method, *J. Comput. Appl. Math.*, **159** (2003), 109–117. https://doi.org/10.1016/s0377-0427(03)00572-7
9. K. Amano, D. Okano, A circular and radial slit mapping of unbounded multiply connected domains, *JSIAM Lett.*, **2** (2010), 53–56. https://doi.org/10.14495/jsiaml.2.53
10. K. Amano, D. Okano, H. Ogata, M. Sugihara, Numerical conformal mappings onto the linear slit domain, *Jpn. J. Ind. Appl. Math.*, **29** (2012), 165–186. https://doi.org/10.1007/s13160-012-0058-0

11. M. Nasser, O. Rainio, A. Rasila, M. Vuorinen, T. Wallace, H. Yu, et al., Polycircular domains, numerical conformal mappings, and moduli of quadrilaterals, *Adv. Comput. Math.*, **48** (2022), 58. https://doi.org/10.1007/s10444-022-09975-x
12. M. M. S. Nasser, A boundary integral equation for conformal mapping of bounded multiply connected regions, *Comput. Methods Funct. Theory*, **9** (2009), 127–143. https://doi.org/10.1007/bf03321718
13. D. Crowdy, The Schwarz-Christoffel mapping to bounded multiply connected polygonal domains, *Proc. R. Soc. A: Math. Phys. Eng. Sci.*, **461** (2005), 2653–2678. https://doi.org/10.1098/rspa.2005.1480
14. D. Crowdy, J. Marshall, Conformal mappings between canonical multiply connected domains, *Comput. Methods Funct. Theory*, **6** (2006), 59–76. https://doi.org/10.1007/BF03321118
15. X. Gu, Y. Wang, T. F. Chan, P. M. Thompson, S. Yau, Genus zero surface conformal mapping and its application to brain surface mapping, *IEEE Trans. Med. Imaging*, **23** (2004), 949–958. https://doi.org/10.1109/TMI.2004.831226
16. X. Gu, F. Luo, S. Yau, Computational conformal geometry behind modern technologies, *Not. Am. Math. Soc.*, **67** (2020), 1509–1525. https://doi.org/10.1090/noti2164
17. H. Hakula, T. Quach, A. Rasila, The conjugate function method and conformal mappings in multiply connected domains, *SIAM J. Sci. Comput.*, **41** (2019), 1753–1776. https://doi.org/10.1137/17M1124164
18. H. Hakula, A. Rasila, Laplace-beltrami equation and numerical conformal mappings on surfaces, *SIAM J. Sci. Comput.*, **47** (2025), 325–342. https://doi.org/10.1137/24M1656840
19. M. M. S. Nasser, Numerical conformal mapping of multiply connected regions onto the fifth category of koebe's canonical slit regions, *J. Math. Anal. Appl.*, **398** (2013), 729–743. https://doi.org/10.1016/j.jmaa.2012.09.020
20. M. M. S. Nasser, Numerical conformal mapping of multiply connected regions onto the second, third and fourth categories of koebe's canonical slit domains, *J. Math. Anal. Appl.*, **382** (2011), 47–56. https://doi.org/10.1016/j.jmaa.2011.04.030
21. T. Wang, D. Huang, G. Ma, Z. Meng, Y. Li, Improved preconditioned conjugate gradient algorithm and application in 3D inversion of gravity-gradiometry data, *Appl. Geophys.*, **14** (2017), 301–313. https://doi.org/10.1007/s11770-017-0625-x
22. C. Vuik, Krylov subspace solvers and preconditioners, in *ESAIM: Proceedings and Surveys*, **63** (2018), 1–43. https://doi.org/10.1051/proc/201863001
23. O. Axelsson, A generalized SSOR method, *BIT Numer. Math.*, **12** (1972), 443–467. https://doi.org/10.1007/bf01932955
24. H. Hakula, A. Rasila, Y. Zheng, The conjugate function method for surfaces with elaborate topological types, preprint, arXiv:2509.01978.

AIMS Press